Statistical Investigation of Radiation-Induced Porosity in BN Fuel Claddings Using Scanning Electron Microscopy

V.I. Pastukhov[1], I.A. Portnykh[1], S.A. Averin[1]

[1]Joint Stock Company "Institute of Nuclear Materials" (INM), Zarechny, Russia

E-mail contact of main author: vladimir.pastukhov91@gmail.com

Abstract. Radiation-induced swelling of claddings is one of the factors limiting service life of fast reactor fuel assemblies. Hydrostatic weighing and transmission electron microscopy are conventional porosity investigation methods.

Hydrostatic weighing is advantageous in terms of the determination radiation porosity integral characteristics, specifically cladding dimensional change after operation in the reactor. However, at low swelling levels (tenths of a percent) the method accuracy is comparable to the measurement error, and its application at the swelling initial stage is ineffective.

Transmission electron microscopy is used to determine quantitative characteristics of radiation porosity, such as size and concentration of radiation-induced voids. One of the main disadvantages of the method is its locality and complexity of sample preparation. High resolution of transmission electron microscope allows observing even small voids (~1 nm) in the foil up to 150 nm thick. Nevertheless, observation of voids exceeding the foil thickness in diameter is complicated, and the reliability of quantitative assessment of large void concentration is quite low.

The paper aims to apply scanning electron microscopy having both method advantages in the radiation porosity investigation. Significant areas of the examined surface together with detection of voids from 10 nm give statistically representative data. Therefore it is possible to obtain information on radiation porosity macroscopic nonuniformity in structural elements subjected to the examination.

The paper presents methodological aspects of radiation porosity investigation with scanning electron microscopy: different modes of sample surface preparation and identification of electron beam optimal parameters. SEM and TEM quantitative results are compared, and radiation porosity nonuniformity in claddings is demonstrated.

Key Words: void swelling, backscattered electron.

1. Introduction

Most often neutron irradiation of metals induces radiation void formation, thereby causing changes of metal volume, as well as different physical and mechanical properties [1-4]. Nowadays radiation-induced porosity investigation techniques may be divided into integrated and local ones. Integrated techniques include hydrostatic weighing and measurement of sample dimensions prior and after irradiation. Transmission electron microscopy (TEM) is the most common local technique. Investigation by transmission electron microscopy detects almost all the range of void sizes with possible quantitative analysis. However, this technique involves some problems with sample preparation – difficulties in remote preparation of thin foil from massive highly active billet. Moreover, small size of the investigated area and low accuracy of its positioning through the billet thickness complicate obtaining statistically representative results and evaluating their macroscopic uniformity.

Conversely, state-of-the art scanning electron microscopes (SEM) may be used to take large field images (e.g., up to hundreds of micrometers or more) with ultimate resolution on the order of ~1 nm [5-9]. Sample preparation for SEM is also much easier than for TEM examination.

2. Materials and procedures

The examination is performed on cladding specimens of fuel elements made of austenitic steel (16Cr-19Ni-2Mo-2Mn-Si-Ti-Nb-V-B) [9-11] after irradiation in fast neutron reactor at different temperatures to different damage doses. SEM examination [12] is carried out using Tescan Mira3 scanning electron microscope with a Schottky Field Emission electron gun. Transmission electron microscopy is performed with JEOL 2000EXII. The TEM sample is prepared by grinding to thin foil, about 130 μm thick, followed by twin-jet electropolishing with 10% HCl and 90% CH_3COOH solutions at 10 °C. SEM examination is carried out on thin foil after TEM and 3x3 mm cross-section segments of fuel cladding. Standard sample is mechanically grinded with Struers TegraPol 15 facility sequentially reducing grain size. Final polishing is made to remove residual surface damage by suspension of colloidal silica.

To investigate distribution of radiation-induced porosity through the cladding thickness a set of 10x10 μm images is taken with backscattered electrons, according to the scheme given in *Fig. 1*. An indent of 10 μm from the section internal surface is made. The distance between imaged areas is about 10 μm as well. As far as cladding thickness is 400 μm, 20 images of radiation-induced porosity are taken. Images are processed with specially developed software SIAMS Photolab.

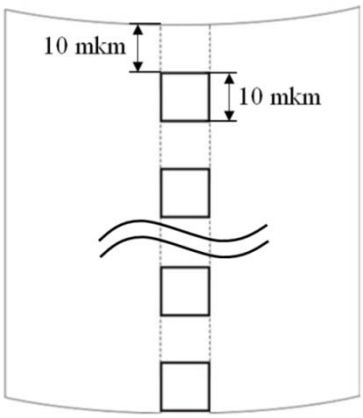

FIG. 1. Imaging scheme for radiation-induced voids through the cladding thickness. Indent from the internal surface made for the first image and further distance between areas are both 10 μm.

Average void diameter for each investigated area should be determined by the formula

$$D_{av} = \frac{\sum_{i=1}^{N} D_i}{N},$$

where D_i is the void diameter, N is the void number in the image.

Radiation-induced voids in the material volume are inhomogeneously distributed, that is related with the structure. To reduce structural factor effect the area of investigated regions is chosen so that its value is comparable with the grain section area. This image area provides sufficient sample volume, close to sampled population of the investigated section.

Standard deviation, displayed in the graph as upper and lower error bars, is used to describe deviation of obtained void diameter values from the average ones.

$$s = \sqrt{\frac{1}{N-1}\left(\sum_{i=1}^{N}(D_i - \overline{D})\right)}$$

3. Results

The paper [13] compares TEM and SEM investigation of radiation-induced porosity. TEM and SEM examination of the same area show not identical, but similar results.

Fig. 2(a) shows a bright field TEM image of EK-164 cladding specimen that had experienced a dose of 87 dpa at a calculated time-averaged temperature of 490 °C. The foil thickness in this area is ~130 nm. In the sample volume voids from 5 to 85 nm are observed.

Fig. 2(b) gives images of the area obtained with scanning electron microscope using backscattered electron detector. *Fig. 2(c)* shows negative SEM image to make it easier to compare with TEM. Small voids (up to 10 nm) distinct in TEM images are almost undetected by SEM. Along with void growth to 30 nm there are close tends in void distribution patterns for TEM and SEM images (*see Fig. 2(d)*).

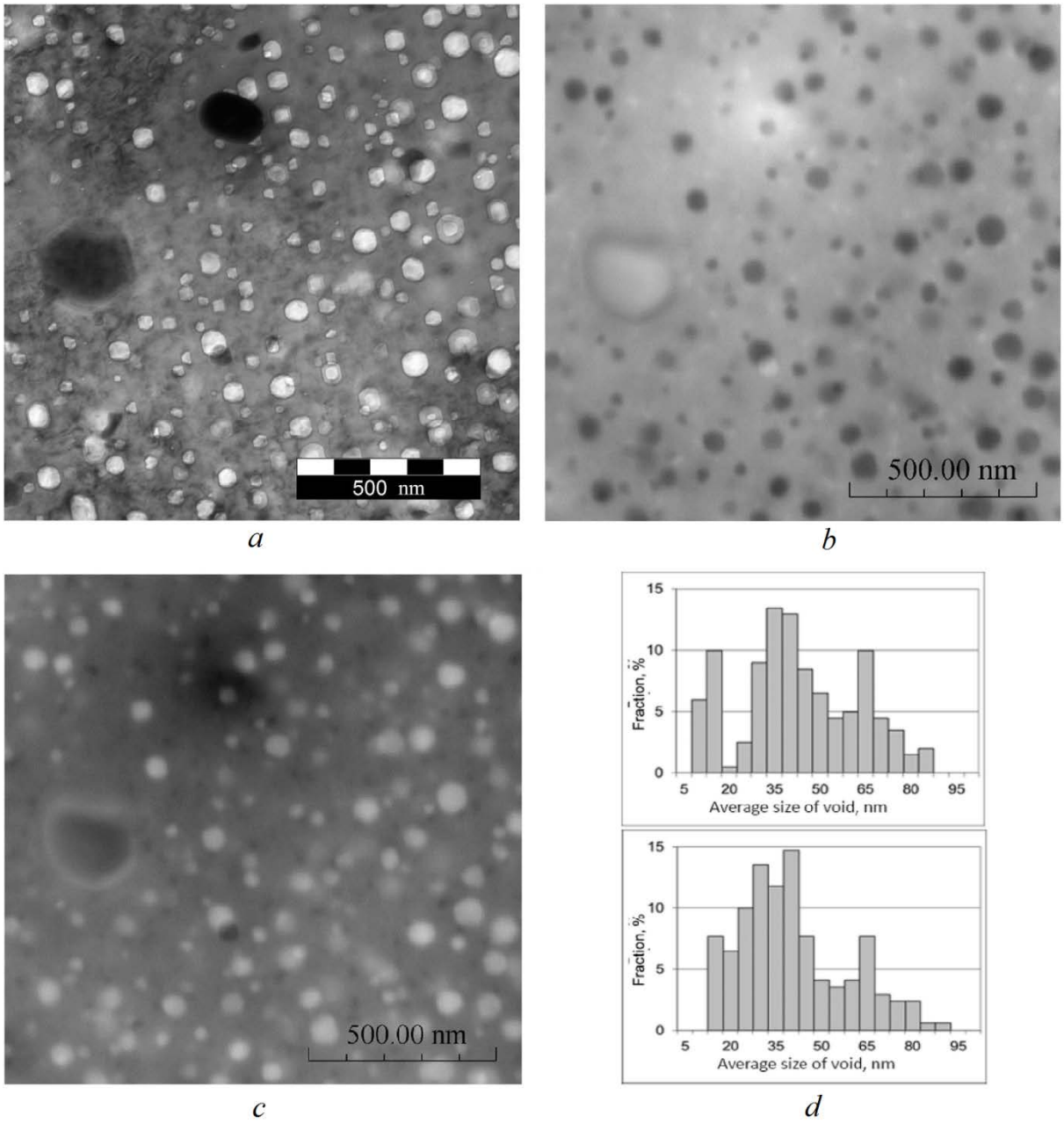

FIG. 2. Comparison of (a) BF TEM and (b) BSE SEM micrographs of the identical field of view of an electron-transparent region from an cladding specimen EK-164 irradiated to 87 dpa at a time-averaged temperature of 490 °C. The micrograph in (c) is an inverted contrast image of the BSE SEM image in (b). Measured void size distributions are shown in (d) for TEM (top) and BSE (bottom) images. The foil thickness in the imaged area is ~130 nm.

Imaging conditions for thin foils ~130 nm thick and bulk samples differ significantly. Experimentally determined in paper [13] optimal parameters for electron beam to investigate radiation-induced porosity of fast reactor specimens with SEM differ from those theoretically predicted in paper [14]. As a result, minimum size of voids detected in *Fig. 3* is 10 nm.

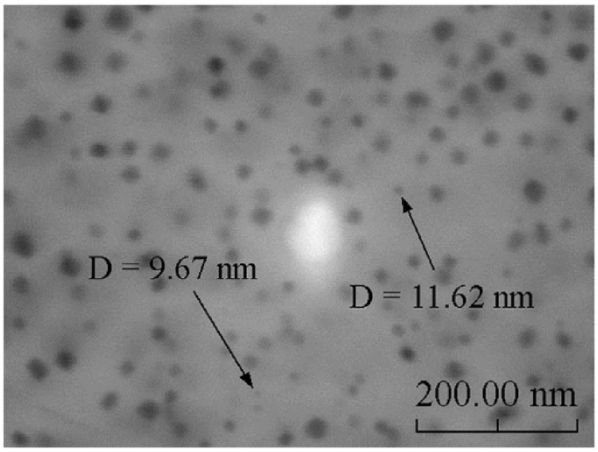

FIG. 3. BSE SEM image of EK-164 sample irradiated to 73 dpa at 475 °C, where the minimum clearly observable void size is ~10 nm. The electron energy is 25 keV and the beam intensity is 13 (arbitrary unit). The white feature in the middle of the micrograph is thought to be a (NbTi)C precipitate of ~100 nm size.

Despite the limit for detected void minimum size SEM is applicable to describe radiation-induced porosity behaviour. Section examination given in paper [13] shows an area depleted in voids up to 8 μm wide at the cladding internal surface (*see Fig. 4(a)*).

In this regard, during examination of radiation-induced void distribution through the cladding thickness a 10 μm indent from the edge is added to the procedure to image the internal cladding surface. There is an area depleted in voids ~8 μm at the internal surface of the specimen irradiated to damage dose of 91.1 dpa at a temperature of 481 °C (*see Fig. 4(a)*). Visual comparison reveals differences in radiation-induced porosity for the regions at the internal (coordinate 10 μm, *Fig. 4(b)*) and external (coordinate 390 μm, *Fig. 4(c)*) surface. At the internal surface larger voids are registered, than those at the external surface, and there is difference in their number per area unit as well.

Processed statistical results of distribution of radiation-induced porosity characteristics through the cladding thickness are given in *Fig. 5*. *Fig. 5a* shows the results of average diameter determination. *Fig. 5b* gives the results of void number determination from the sample images. There are more than 6000 voids for 100 μm^2 at the internal surface, 10 μm from the external one (*see Fig. 4b*). It can be seen from the graph that smooth reduction of the average void size is registered from the internal surface to the external one. Thus at the external surface (*see Fig. 5c*) there are about 12000 voids for the investigated area. Along with average size reduced void number per area unit tends to increase. Average size and void number vary, perhaps, due to structural elements of austenitic steels. Average void diameter variation from the internal surface to the external one is related with temperature gradient through the cladding thickness.

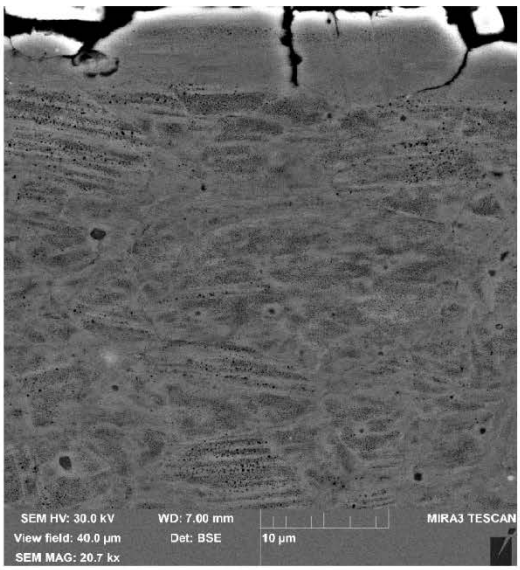

a

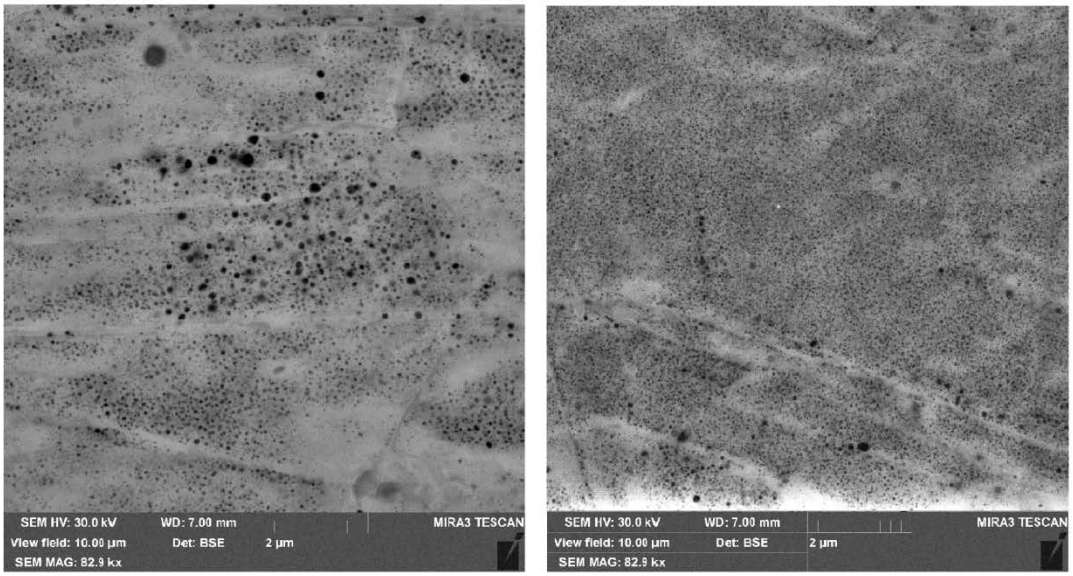

b *c*

FIG. 4. End section of the cladding irradiated to 91.1 dpa at a temperature of 481 °C at the internal surface (a). An area with the examined radiation-induced porosity at coordinates of 10 µm (b) and 390 µm (c).

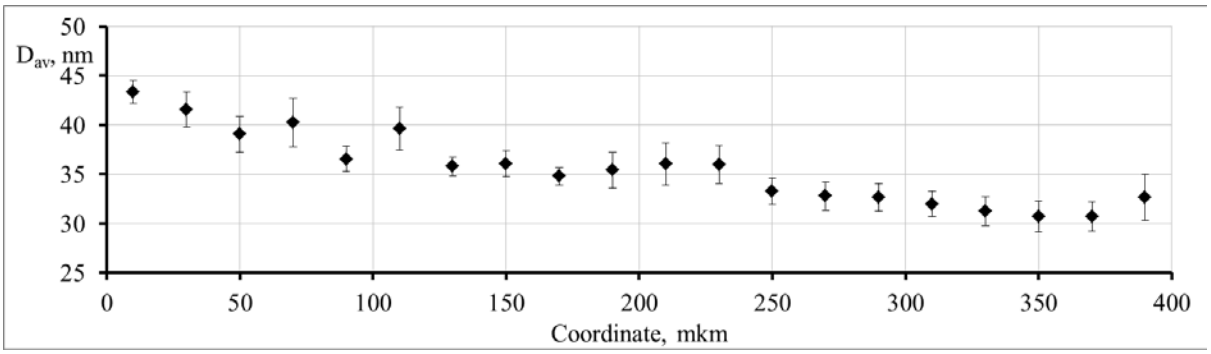

a

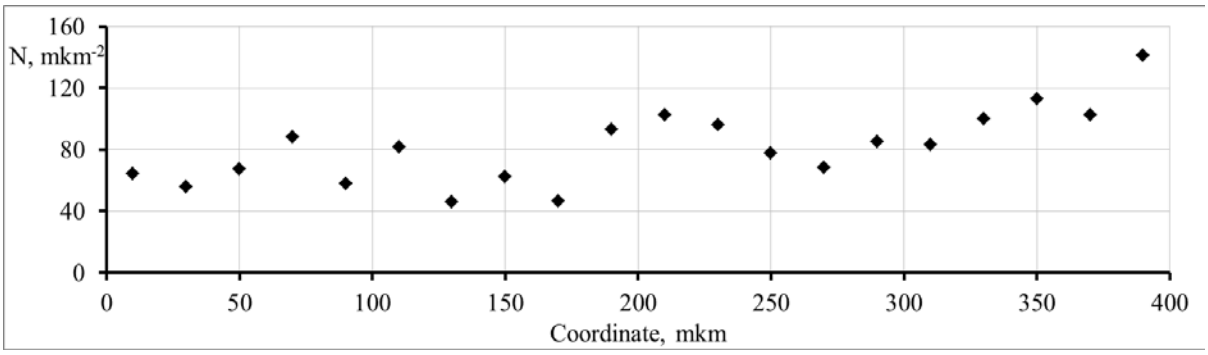

b

FIG. 5. Diagram of average void size (a) and void number (b) variation through thickness of the cladding irradiated to 91.1 dpa at a temperature of 481 °C.

4. Conclusion

It has been demonstrated that back-scattered electrons can be used in a scanning electron microscope to image a very wide field of view of metal specimens containing radiation-induced cavities, especially those large enough to be considered to be voids. It has been demonstrated that back-scattered electrons can be used in a scanning electron microscope to image a very wide field of view of metal specimens containing radiation-induced cavities, especially those large enough to be considered to be voids. There are some limitations on this imaging technique involving the size of the smallest cavities and the depths over which they can be reliably imaged.

5. References

[1] GARNER, F.A. Radiation damage in austenitic steels, in: R.J.M. Konings (Ed.), Comprehensive Nuclear Materials, vol. 4, Elsevier, 2012, pp. 33-95.

[2] KOZLOV, A.V., SHCHERBAKOV, E.N., AVERIN, S.A., GARNER, F.A., “The effect of void swelling on electrical resistance and elastic moduli in austenitic steels”, in: M.L. Grossbeck, T.R. Allen, R.G. Lott, A.S. Kumar (Eds.), Effects of Radiation on Materials, ASTM STP 1447, ASTM International, West Conshohocken PA (2004), 66–77.

[3] BALACHOV, I.I., SHCHERBAKOV, E.N., KOZLOV, A.V., PORTNYKH, I.A., GARNER, F.A. “Influence of irradiation-induced voids and bubbles on physical properties of austenitic structural alloys”, J. Nucl. Mater. 329–333 (2004) 617–620.

[4] GARNER, F.A., KOZLOV, A.V., OKITA, T. “The Competing Influences of Void Swelling and Radiation-induced Precipitation on Dimensional Stability and Thermalphysical Properties of Austenitic Stainless Steels in PWR and VVER Internals”, Proc. 17th International Conference on Environmental Degradation of Materials in Nuclear Power Systems & Water Reactors, Ottawa, Ontario, Canada (2015).

[5] SHIMIZU, K., MITANI, T., New Horizons of Applied Scanning Electron Microscopy, Springer (2009), http://www.springer.com/series/409.

[6] GOLDSTEIN, Joseph I., et al., Scanning Electron Microscopy and X-Ray Microanalysis, third ed., Kluwer Academic/Plenum Publishers, New York (2003).

[7] ROUSSEL, Laurent Y., STOKES, Debbie J., GESTMANN, Ingo, DARUS, Mark, YOUNG, Richard J., Extreme high resolution scanning electron microscopy (XHR SEM) and beyond, in: Proceedings of SPIE e the International Society for Optical Engineering, 05/2009, http://dx.doi.org/10.1117/12.821826.

[8] DUDAREV, S.L., REZ, P., WHELAN, M.J. Theory of electron backscattering from crystals, Phys. Rev., B 51 (1995) 3397.

[9] BAKANOV, M.V. et al. The main results of structural materials operation in BN-600 reactor core. Izvestia visshikh uchebnikh zavedeniy, Yadernaya energetika, No. 1 (2011), 177-186 (in Russian).

[10] TSELISHCHEV, A.V., BUDANOV, Yu.P., MITROFANOVA, N.M. et al. Development of core structural steels for BN reactors based on post-irradiation examination results. Atomnaya Energiya, No. 108, Vol. 4 (2010), 217-221 (in Russian).

[11] AGEEV, V.S. et al. Core structural materials for Russian fast reactors. Status and prospects. Izvestia visshikh uchebnikh zavedeniy, Yadernaya energetika, No. 2 (2009), 210-218 (In Russian).

[12] SINELNOKIV, L.P. et al. Equipment and techniques for post-irradiation examination of materials at JSC “INM” hot cell laboratory. Atomnaya Energiya, No. 121, Vol. 4 (2016), 187-194 (in Russian).

[13] PASTUKHOV, V.I., AVERIN, S.A., PANCHENKO, V.L., PORTNYKH, I.A., FREYER, P.D., GIANNUZZI, L.A., GARNER, F.A. Application of backscatter electrons for large area imaging of cavities produced by neutron irradiation, Journal of Nuclear Materials 480 (2016) 289–300.

[14] YAN, Qiang, GIGAX, Jonathan, CHEN, Di, GARNER, F.A., SHAO, Lin. Monte Carlo modeling of cavity imaging in pure iron using backscatter electron scanning microscopy, Journal of Nuclear Materials 480 (2016) 420–428.